LANGMUIR

pubs.acs.org/Langmuir Article

High-Performance Ultrafine Bubble Aeration on Janus Aluminum Foil Prepared by Laser Microfabrication

Jianping Tang,[‖] Yachao Zhang,[‖] Yansheng Yao,* Nianwei Dai, Zhangsen Ge, and Dong Wu*

Cite This: *Langmuir* 2021, 37, 6947−6952 Read Online

ACCESS | Metrics & More | Article Recommendations | Supporting Information

ABSTRACT: Aeration is a mass transfer process, in which gas is dispersed into a liquid by utilizing air inflation or agitation. Typically, a microporous device is often used for aeration. Increasing the gas flow rate and decreasing the pore size reduce the bubble size, but the surface wettability of the gas/solid interface also has a significant impact on the bubble size, which is rarely studied. In this study, a superhydrophilic/superhydrophobic Janus aluminum foil (JAF) is fabricated by laser microstructuring and low surface energy modification. The gas-repelling superhydrophilic surface not only facilitates ultrafine bubble generation but also allows the bubbles to detach from the aerator surface quickly, while the superhydrophobic surface prevents water from infiltrating into the aeration chamber and reduces the mass transfer resistance. The micropores with different diameters are obtained by adjusting the laser processing parameters. The pore prepared by the laser is uniform, consequently leading to the uniform bubble size. When the pore diameter is set to 30 μm, the diameter of bubbles released from the superhydrophilic surface of the JAF is only 0.326 mm, and the gas dissolution rate is about six times that of the double-sided superhydrophobic aluminum foil. This simple, low-cost, and controllable method of the laser processing JAF has broad applications in wastewater treatment, energy production, and aquaculture.

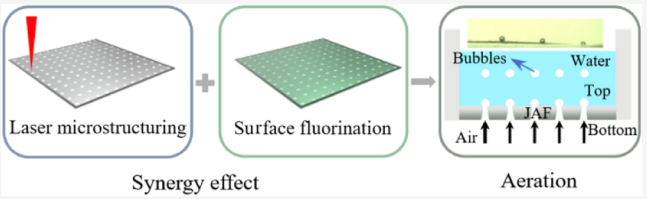

INTRODUCTION

Bubble aeration is a means of strong contact between air and water. Its purpose is to rapidly dissolve oxygen into water or to discharge unwanted gases and volatile substances into the air to improve the water environment.[1] As the bubble size decreases, the gas/liquid contact area increases, and thus, the gas/liquid mass transfer efficiency is enhanced.[2] At present, fine bubbles can be obtained mainly through jet aeration,[3] mechanical aeration,[4] and micropore aeration.[5] Compared with other aeration methods, micropore aeration is widely used by virtue of its lower cost and simplicity during manufacturing. The traditional micropore aeration methods are mostly based on the porous glass membrane,[6] porous ceramic membrane,[7] and hollow fiber membrane.[8] However, due to the limitation of the preparation process, the fabricated pores are randomly distributed with various pore sizes, resulting in a wide distribution of the bubble sizes.

In nature, the top surface of the lotus leaf is superhydrophobic and the bottom surface is superhydrophilic, which is defined as the Janus surface.[9] In recent years, Janus membranes with asymmetric surface wettability have shown broad applications in solar water purification,[10−12] directional water transport,[13−15] oil-water separation,[16−18] fog collection,[19−21] and tissue regeneration.[22,23] Yang et al. first developed the Janus membrane with asymmetric wettability for fine bubble aeration. The hydrophobic porous polypropylene membrane was partially immersed in the polydopamine/polyethyleneimine solution to achieve hydrophilicity on one side. Compared with the hydrophobic membrane, the size of bubbles formed by the Janus membrane is reduced from 4 to 0.5 mm and oxygen dissolves more quickly.[5] Wang et al. prepared the Janus membrane by simply spraying polydopamine on the surface of the polypropylene membrane for dye adsorption and microbubble aeration.[24] However, due to the randomly distributed pores with various sizes of the porous membrane used in these studies, bubble coalescence emerged and large bubbles were still formed. In this regard, seeking a facile and low-cost way to prepare a uniform micropore surface with asymmetric wettability for fine bubble aeration is still an urgent need.

Because of high precision and good controllability, laser surface texturing has been used to tailor surface properties for various applications such as condensation,[25] boiling,[26] tribology,[27] cavitation,[28] and icing prevention.[29] Herein, we prepare a Janus aluminum foil (JAF) with a uniform micropore array by laser processing and low surface energy modification. The gas-repelling superhydrophilic surface is beneficial to reducing the bubble size and accelerating the detachment of bubbles from the aluminum foil surface, while the superhydrophobic surface

Received: February 13, 2021
Revised: May 14, 2021
Published: June 1, 2021

https://doi.org/10.1021/acs.langmuir.1c00437
Langmuir 2021, 37, 6947−6952

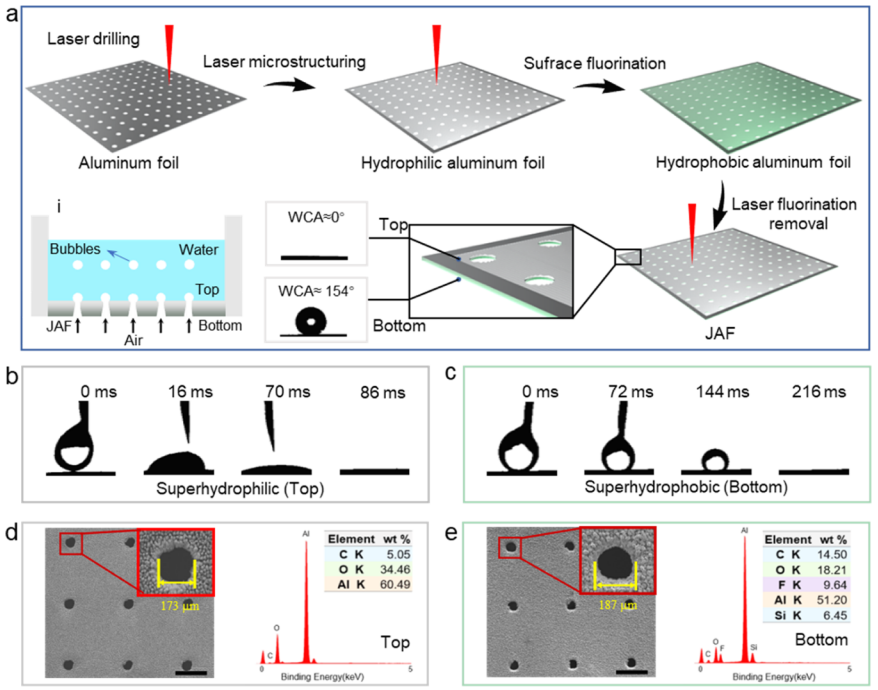

Figure 1. Preparation and characterization of the JAF. (a) Schematic of the preparation of the porous JAF by laser processing and low surface energy modification. Inset: The superhydrophilic side of the JAF is placed on the top in the aerator to generate ultrafine bubbles. (b) Water droplet spreading out on the superhydrophilic side of the porous JAF. (c) Water droplet spontaneously penetrating from the superhydrophobic side of the porous JAF to the superhydrophilic side quickly. (d) SEM images and EDS result of the superhydrophilic side of the JAF. (e) SEM images and EDS result of the superhydrophobic side of the JAF. The scale bars in (d,e) are 500 μm.

prevents water from infiltrating into the aeration chamber and greatly reduces the mass transfer resistance. Uniform and ultrafine bubble aeration for a long time is achieved by adjusting micropore diameter and pore spacing. The proof-of-concept demonstration of the JAF for improving the gas dissolution rate is performed by a color indication experiment. The high-performance JAF fabricated by the laser possesses the advantages of simple fabrication and low cost, suggesting a promising application in more fields of micropore aeration.

RESULTS AND DISCUSSION

The fabrication process of the microporous array of the JAF is shown in Figure 1a. First, a uniform micropore array with the pore spacing of 1 mm is prepared by laser drilling on the aluminum foil surface. Second, the surface is processed by laser microstructuring to increase its roughness. Afterward, the aluminum foil is modified with 1*H*,1*H*,2*H*,2*H*-perfluorodecyltriethoxysilane (PFDTES). Due to the synergistic effect of the rough microstructure and low surface energy chemical property, the surface shows superhydrophobicity (water contact angle is 154°) and underwater superaerophilicity (bubble contact angle is 0°, Figure S1). At last, the top surface of the aluminum foil is ablated by laser processing and the intrinsic hydrophilic aluminum foil is exposed. The water contact angle of the top surface is nearly 0°, and thus, the JAF is obtained. Because water occupies the superhydrophilic surface, the bubble cannot adhere to the surface, finally leading to superaerophobicity. When the JAF is placed in water, a mirror-like air layer can be found only on the superhydrophobic surface (Figure S1).

The porous JAF is placed in the aerator with the superhydrophilic side on the top, and the gas enters the aqueous solution through the JAF to form bubbles, as schematically shown in Figure 1a. A 4 μL droplet is dropped onto the superhydrophilic surface, and the droplet spreads rapidly on the surface within 86 ms (Figure 1b). When the aluminum foil is flipped and a 4 μL droplet is added to the superhydrophobic surface, the droplet volume gradually decreases and permeates through the superhydrophilic side within 216 ms (Figure 1c). The pores fabricated by laser are conical (Figure S2). The smaller openings are at the top (Figure 1d,a) and the larger openings are at the bottom (Figure 1e,a), which are 173 ± 2 μm and 187 ± 3 μm, respectively. According to the energy-dispersive X-ray spectroscopy (EDS) elemental analysis, it can be seen that the F element appears on the superhydrophobic surface of the sample after PFDTES modification, which confirms the effect of low surface energy modification. The F element disappears at the superhydrophilic surface after laser ablation, which further confirms the effect of laser surface modification.

To study the synergistic effect of surface wettability and pore size on the bubbling behavior, we build an aerator device by using a commercial air pump to supply gas. A large number of ultrafine bubbles rise in water as the gas passes through the JAF, while a small number of large bubbles are formed in water as the gas passes through the HBAF (Figure S3), which are captured by a high-speed camera. To facilitate observation and measurement, five pores in a row with 2.5 mm spacing are fabricated on the aluminum foil surface. Figure 2a,d shows the scanning electron microscopy (SEM) images of the aluminum foil surfaces with pore diameters of 30 and 180 μm, respectively. Figure 2b,e shows the bubbling process of the JAF with pore diameters of 30 and 180 μm, respectively. Typical spherical ultrafine bubbles are produced, when the gas passes through the superhydrophilic surface of the JAF. The average bubble diameter is 0.326 mm for 30 μm and 1.94 mm for 180 μm pores. Correspondingly, the time from bubble generation to

https://doi.org/10.1021/acs.langmuir.1c00437
Langmuir 2021, 37, 6947−6952

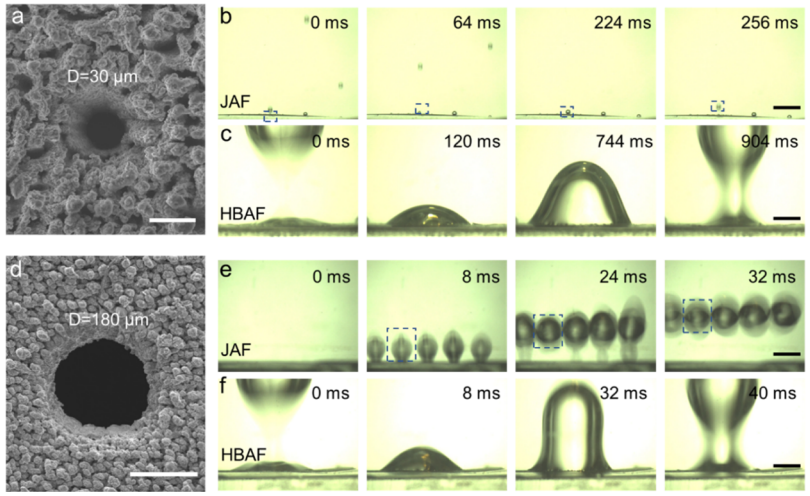

Figure 2. Bubbling behavior of the JAF and HBAF with different pore sizes. (a,d) SEM images of the aluminum foil surfaces with pore diameters of 30 and 180 μm, respectively. (b) JAF and (e) HBAF with a pore diameter of 30 μm. (c) JAF and (f) HBAF with a pore diameter of 180 μm. Scale bars: 20 μm (a), 200 μm (d), and 2.5 mm (b–c,e–f).

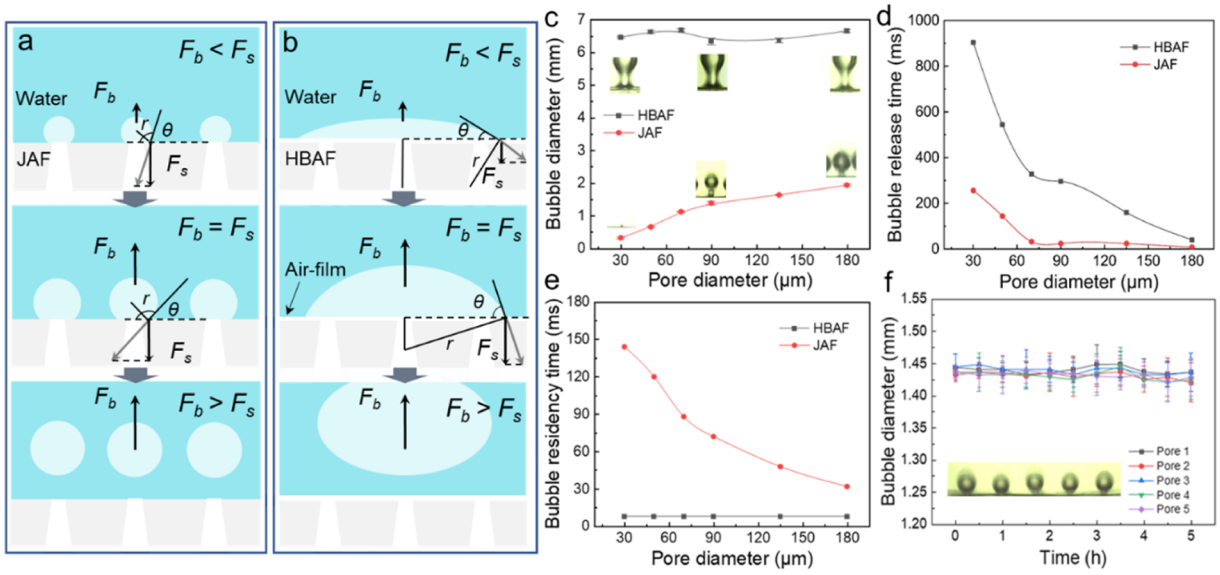

Figure 3. Schematic interpretation of forces acting on the bubble at different stages for (a) JAF and (b) HBAF. The quantitative relationship of the (c) bubble diameter, (d) bubble release time, and (e) bubble residency time with the aluminum foil pore size. (f) Bubble uniformity and long-time stability characterization of the JAF. The inset in (f) is the image of the five bubbles generated from the five pores at 5 h, and the pore diameter is 90 μm.

release is 256 and 32 ms, respectively. Compared with the Janus membrane made of porous polypropylene[5] and other reported works, the bubbles we produced exhibit a smallest size (Table S1). In the case of much smaller pores and extremely low porosity on the surface of the aluminum foil, the gas intrusion pressure is too large, resulting in unstable gas/liquid mass transfer, and some pores cannot produce bubbles (Figure 2b).

Figure 2c,f shows the bubbling process of the HBAF with pore diameters of 30 and 180 μm, respectively. When the gas passes through the superhydrophobic surface of the HBAF, a single and large hemispherical bubble is generated. The average bubble diameter is almost the same for two pore diameters (6.47 mm for 30 μm pore and 6.66 mm for 180 μm pore) after the bubble is completely detached from the surface of the HBAF. Correspondingly, the bubble release times are 904 and 40 ms, respectively. As for the JAF with a 90 μm pore, the bubble diameter is 1.43 mm and the bubble release time is 24 ms. In contrast, the bubble diameter is 6.44 mm for the HBAF with a 90 μm pore and its bubble release time is 296 ms (Figure S4). In addition, for the double-sided superhydrophilic aluminum foil, water penetrates easily into the pores and the gas intrusion pressure increases. Moreover, in the case of no gas supply, water directly penetrates the aluminum foil to the aeration chamber, consequently causing great difficulties to the aeration experiment (Movie S1).

Figure 3a,b presents the schematic interpretation of the forces acting on the bubble at different stages on the surface of the JAF and HBAF, respectively. The bubble is mainly subjected to buoyancy F_b and surface adhesion force F_s (an axial component of surface tension).[16] Because the bubble rises vertically along the pore, the influence of the radial component of surface tension can be ignored. Besides, the density of the gas is much lower compared with liquids, and so, the effect of bubble gravity can be ignored.[30] With the continuous growth of the bubble, the buoyancy overcomes surface adhesion that prevents the bubble from detaching, and the bubble begins to detach from the

https://doi.org/10.1021/acs.langmuir.1c00437
Langmuir 2021, 37, 6947–6952

surface of the aluminum foil.[31] It is assumed that the bubble is spherical and F_b is expressed by eq 1. For both types of the aluminum foil, the buoyancy increases with the increase in bubble size following the relationship $F_b \propto r^3$. F_s also changes with the growth of bubbles, and F_s can be expressed by eq 2.[30]

$$F_b = \rho g \frac{4}{3}\pi r^3 \quad (1)$$

$$F_s = 2\pi(r \sin\theta)\gamma \sin\theta \quad (2)$$

where ρ is the density of water, g is the gravitational acceleration, r refers to the radius of the bubble, γ stands for the surface tension of water, θ means the bubble contact angle, and $2\pi(r \sin\theta)$ shows the length of the three-phase contact line (TPCL). For the gas-repelling property of the superhydrophilic surface of the JAF, the TPCL is relatively short and hard to move, and thus, the bubble contact angle mainly increases and F_s decreases. F_b increases with r^3, and so, the bubble quickly detaches from the surface of the JAF and the bubble size is small. As the TPCL length of the JAF decreases with the pore size, the bubble size decreases, and the minimum size is 0.326 mm (Figure 3c). On the contrary, due to the superaerophilicity of the HBAF, the TPCL is easy to expand (Figure 3b). The bubbles formed on the HBAF can cross multiple micropores and merge with the neighboring bubbles on its surface.[32] Therefore, the bubble contact radius increases sharply and F_s increases. When F_b increases enough to exceed F_s, a large bubble detaches from the HBAF. The final released bubble size is irrelevant to the pore size, and the average bubble diameter reaches 6.47 mm (Figure 3c). It is worthy to note that the pore spacing also has an influence on the bubble size. As shown in Figure S5, for the HBAF with a 70 μm pore, when the pore spacing is 2.5 mm, the bubble 1 and bubble 2 coalesce into a large bubble within 16 ms owing to the easy movement property of the TPCL. As shown in Figure S6, for the case of the JAF with the same pore size, even when the pore spacing is as small as 1 mm, the bubbles still do not coalesce. As the pore spacing decreases to 0.5 mm, the bubble coalesces with the neighboring bubble. Therefore, in order to obtain ultrafine bubbles, it is necessary that the surface of the porous membrane is superaerophobic in the liquid and has an appropriate pore spacing.

Bubble release time is also important for aeration. The faster the bubble release speed is, the higher will be the mass transfer efficiency. However, the bubble release time is rarely studied in previous studies. Figure 3d shows that the bubble release time decreases with the pore size. For the JAF, the larger the pore is, the larger the bubble will be. As mentioned above, the buoyancy ($F_b \propto r^3$) increases much faster than the surface adhesion force ($F_s \propto r$), and thus, the bubble is easier to detach from the surface as the bubble size increases. The bubble release time decreases from 256 to 32 ms when the pore diameter increases from 30 to 180 μm. For the HBAF, the larger the pore is, the more gas is supplied, and the faster the TPCL migration is and the earlier will be the bubble release. The bubble release time is reduced from 904 to 40 ms when the pore diameter increases from 30 to 180 μm. It can be seen that both the surface wettability and pore size of the aluminum foil play a vital role in the size and the release time of bubbles.

The longer the time for bubble to stay in the liquid (the bubble residency time) is, the higher will be the mass transfer efficiency. The bubble residency time in the liquid is greatly extended, as the bubble size decreases.[2,33] The bubbles produced by the HBAF are large and have similar sizes for different pores, and these bubbles stayed in the liquid for less than 8 ms. The ultrafine bubbles produced by the JAF have a longer residency time. As the bubble diameter decreases with the pore size, the maximum residency time is 144 ms for a 30 μm pore (Figures 3e and S7).

To explore the size uniformity of the ultrafine bubbles generated from the JAF, five pores with a 90 μm diameter are fabricated. The gas is continuously inflated through the JAF for 5 h, and the diameters of the generated bubbles are measured every half an hour. As shown in Figure 3f, the diameters of the bubbles produced in all five pores are the same and remain unchanged for 5 h, demonstrating the stability of the fabricated JAF in aeration. The JAF is then sealed in the plastic bag at room temperature of 19 °C and relative humidity of 35%. 4 months later, the same JAF was tested under aeration conditions for 24 h, and the diameter of the bubble was measured every 4 h. The results show that the bubbles produced by the JAF have the same size as 4 months ago and have good uniformity (Figure S8). The JAF with a pore of 30 μm is also tested under aeration conditions for 24 h, and the bubble size could maintain ~0.326 mm (Figure S9).

To quantitatively compare the gas dissolution rate, CO_2 is inflated through the JAF and HBAF into the bromothymol blue solution, (Figure 4a). The pore diameter of both aluminum foils is 30 μm, and the pore spacing is 1 mm. In regard to the JAF, with the continuous supply of CO_2 gas, dense and ultrafine bubbles are generated from the superhydrophilic surface. For these ultrafine bubbles, both the bubble residency time and the gas/liquid contact area are dramatically increased in water, and thus, the solution pH value is rapidly decreased. The blue solution turns green quickly and finally turns yellow in 10 s (Figure 4b, Movie S2). In contrast, in the case of the HBAF with the same condition of the CO_2 gas flow rate, a large bubble is generated in sequence with a long period, and the rising speed is fast. Thus, the solution pH value is slowly decreased, and the entire reaction time for the HBAF is 54 s, which is almost six times that of the JAF (Figure 4c, Movie S2). The lower/higher pore spacing values are also tested; because the bubble diameter is much smaller than the pore spacing of 1.5 mm, the adjacent bubbles are not merged, and the gas dissolution rate is similar to that when the pore spacing is 1 mm. Differently, the bubble diameter is larger than the pore spacing of 0.1 mm, the adjacent bubbles merge, and the gas dissolution rate decreases (Figure S10).

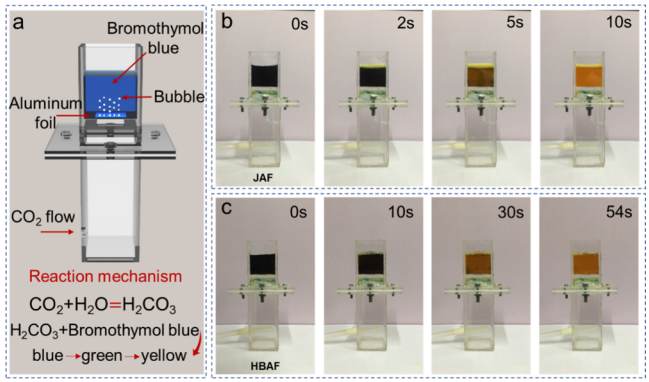

Figure 4. Comparison of the gas dissolution rate between the JAF and the HBAF through the bromothymol blue color indication experiment. (a) Schematic of aeration. The carbon dioxide gas is introduced with the same gas flow rate. (b) JAF and (c) HBAF.

https://doi.org/10.1021/acs.langmuir.1c00437
Langmuir 2021, 37, 6947−6952

CONCLUSIONS

In summary, a method of laser processing combined with low surface energy modification is proposed to fabricate a JAF (superhydrophilic/superhydrophobic) with asymmetric wettability for ultrafine bubble aeration. By controlling the morphology of the pores and wettability of the aluminum foil, ultrafine and uniform bubble aeration with long time stability is achieved. Compared with the HBAF, the JAF exhibits higher gas utilization, which is verified by the bromothymol blue color indication experiment. The proposed method shows great potential in the areas of increasing oxygen in water bodies, separating algae from water bodies, strengthening the oxidative decomposition of ozone, and enhancing biological activity.

EXPERIMENTAL SECTION

Materials. The aluminum foil (Saiwei Precision Metal Materials Co., Ltd) has a purity of 99.9%, a thickness of 0.1 mm, and an area of 3 × 3 cm^2. The bromothymol blue solution is purchased from Creative Science and Education Company. PFDTES is purchased from Aladdin Company.

Fabrication of the Porous Aluminum Foil. The laser used is the ytterbium-doped pulsed fiber laser system (JPTYDFLP-60), and the laser spot diameter is 27 μm. In the laser drilling process, the laser power, frequency, pulse width, processing number, and scanning speed are set to 13 W, 320 KHz, 10 ns, 120 times, and 20 mm/s, respectively. In the laser microstructuring process, the laser power, frequency, pulse width, processing number, and speed used are set to 5 W, 150 KHz, 10 ns, 1 time, and 50 mm/s, respectively, and the scanning spacing is 20 μm. The double-sided superhydrophilic aluminum foil, HBAF, and JAF (superhydrophobic/superhydrophilic) are all composed of a uniform array of micropores, the spacing of the micropore array is 1 mm, and the pore diameters are 30, 50, 70, 90, 135, and 180 μm, respectively. Both sides of the superhydrophilic porous aluminum foil are ablated by the laser to form rough microstructures. The PFDTES solution is mixed with ethanol at a mass ratio of 1: 85 at room temperature, and then, the mixed solution is thoroughly stirred. The aluminum foil is immersed in the dilute PFDTES solution for 12 h and dried in an oven at 80 °C for 15 min, and the HBAF is prepared. After single-sided laser scanning of the HBAF, the fluorine substance on the top surface is removed and the JAF is obtained.

Instrument and Characterization. The contact angles of 4 μL deionized water droplets and 4 μL bubbles at different positions are measured with a contact angle meter (CA100D, Innuo, China), and the average value is obtained. The surface morphology of the microporous array aluminum foil is characterized by field-emission scanning electron microscopy (SEM, JSM-6700F, JEOL, Tokyo, Japan). The high-speed camera with a frame rate of 120 frames/s is used to record the bubbling process. The aluminum foil is placed underwater at the depth of 2.8 cm. The height of the camera's field of view is 8 mm, and the bubble residency time is obtained by measuring the time it takes for the bubble to rise out of the field of view.

Aeration Experiment. The aluminum foil and the aerator are sealed with a double-sided tape, and the top surface of the aluminum foil is in direct contact with the bromothymol blue solution. The 10 × 10 pore array with a pore diameter of 30 μm is fabricated, and the pore spacing is 1 mm.

ASSOCIATED CONTENT

Supporting Information

The Supporting Information is available free of charge at https://pubs.acs.org/doi/10.1021/acs.langmuir.1c00437.

Each side of the JAF showing different air affinity behaviors under the underwater condition, SEM images, different bubbling behaviors on the surface of JAF and HBAF with the same gas flow rate, and bubble coalescence behavior at different pore spacing in JAF and HBAF, comparison of bubble diameters, influence of pore spacing, bubble residency time, bubble uniformity and long-time stability characterization, and comparison of the gas dissolution rate (PDF)

Penetration of the liquid through the superhydrophilic aluminum foil under no gas supply conditions (MP4)

Comparison of the gas dissolution rate by the bromothymol blue solution color indication test between the JAF and the HBAF (MP4)

AUTHOR INFORMATION

Corresponding Authors

Yansheng Yao − *School of Mechanical and Electrical Engineering, Anhui Jianzhu University, Hefei, Anhui 230601, China; Key Laboratory of Intelligent Manufacturing of Construction Machinery, Hefei, Anhui 230601, China*; Email: y.ys@163.com

Dong Wu − *CAS Key Laboratory of Mechanical Behavior and Design of Materials, Department of Precision Machinery and Precision Instrumentation, University of Science and Technology of China, Hefei, Anhui 230026, China*; orcid.org/0000-0003-0623-1515; Email: dongwu@ustc.edu.cn

Authors

Jianping Tang − *School of Mechanical and Electrical Engineering, Anhui Jianzhu University, Hefei, Anhui 230601, China*; orcid.org/0000-0003-0069-7621

Yachao Zhang − *CAS Key Laboratory of Mechanical Behavior and Design of Materials, Department of Precision Machinery and Precision Instrumentation, University of Science and Technology of China, Hefei, Anhui 230026, China*

Nianwei Dai − *CAS Key Laboratory of Mechanical Behavior and Design of Materials, Department of Precision Machinery and Precision Instrumentation, University of Science and Technology of China, Hefei, Anhui 230026, China*

Zhangsen Ge − *School of Mechanical and Electrical Engineering, Anhui Jianzhu University, Hefei, Anhui 230601, China*

Complete contact information is available at: https://pubs.acs.org/10.1021/acs.langmuir.1c00437

Author Contributions

‖J.T. and Y.Z. contributed equally to this work.

Notes

The authors declare no competing financial interest.

ACKNOWLEDGMENTS

This work was supported by the National Natural Science Foundation of China (nos. 61927814, 51875544, 51675503, and 91963127), National Key R&D Program of China (2017YFB1104303), Major Scientific and Technological Projects in Anhui Province (201903a05020005), the Fundamental Research Funds for the Central Universities (YD209000205, WK6030000108, WK5290000001, and WK2090050048), and the Youth Innovation Promotion Association CAS (2017495). We acknowledge the Experimental Center of Engineering and Material Sciences at USTC for the fabrication and measurement of samples. This work was partly carried out at the USTC Center for Micro and Nanoscale Research and Fabrication.

https://doi.org/10.1021/acs.langmuir.1c00437
Langmuir 2021, 37, 6947−6952

REFERENCES

(1) Yang, H.-C.; Xie, Y.; Hou, J.; Cheetham, A. K.; Chen, V.; Darling, S. B. Janus Membranes: Creating Asymmetry for Energy Efficiency. *Adv. Mater.* **2018**, *30*, 1801495.

(2) Shi, X.; Xue, S.; Marhaba, T.; Zhang, W. Probing Internal Pressures and Long-Term Stability of Nanobubbles in Water. *Langmuir* **2021**, *37*, 2514−2522.

(3) Guo, L.; Liu, W.; Tang, X.; Wang, H.; Liu, Q.; Zhu, Y. Reaction kinetics of non-catalyzed jet aeration oxidation of magnesium sulfite. *Chem. Eng. J.* **2017**, *330*, 870−879.

(4) Yang, Z.; Cheng, J.; Liu, J.; Zhou, J.; Cen, K. Improving microalgal growth with small bubbles in a raceway pond with swing gas aerators. *Bioresour. Technol.* **2016**, *216*, 267−272.

(5) Yang, H.-C.; Hou, J.; Wan, L.-S.; Chen, V.; Xu, Z.-K. Janus Membranes with Asymmetric Wettability for Fine Bubble Aeration. *Adv. Mater. Interfaces* **2016**, *3*, 1500774.

(6) Kukuzaki, M.; Fujimoto, K.; Kai, S.; Ohe, K.; Oshima, T.; Baba, Y. Ozone mass transfer in an ozone-water contacting process with Shirasu porous glass (SPG) membranes-A comparative study of hydrophilic and hydrophobic membranes. *Sep. Purif. Technol.* **2010**, *72*, 347−356.

(7) Li, Q.; Jia, R.; Shao, J.; He, Y. Photocatalytic degradation of amoxicillin via TiO2 nanoparticle coupling with a novel submerged porous ceramic membrane reactor. *J. Cleaner Prod.* **2019**, *209*, 755−761.

(8) Wang, B.; Xiong, X.; Shui, Y.; Huang, Z.; Tian, K. A systematic study of enhanced ozone mass transfer for ultrasonic-assisted PTFE hollow fiber membrane aeration process. *Chem. Eng. J.* **2019**, *357*, 678−688.

(9) Koşak Söz, Ç.; Trosien, S.; Biesalski, M. Superhydrophobic Hybrid Paper Sheets with Janus-Type Wettability. *ACS Appl. Mater. Interfaces* **2018**, *10*, 37478−37488.

(10) Zhao, Q.; Du, C.; Jia, Y.; Yuan, J.; Song, G.; Zhou, X.; Sun, S.; Zhou, C.; Zhao, L.; Yang, S. Solar-powered Janus membrane for one-step conversion of sewage to clean water. *Chem. Eng. J.* **2020**, *387*, 124131.

(11) Xu, W.; Hu, X.; Zhuang, S.; Wang, Y.; Li, X.; Zhou, L.; Zhu, S.; Zhu, J. Flexible and Salt Resistant Janus Absorbers by Electrospinning for Stable and Efficient Solar Desalination. *Adv. Energy Mater.* **2018**, *8*, 1702884.

(12) Yang, Y.; Yang, X.; Fu, L.; Zou, M.; Cao, A.; Du, Y.; Yuan, Q.; Yan, C.-H. A Two-Dimensional Flexible Bilayer Janus Membrane for Advanced Photothermal Water Desalination. *ACS Energy Lett.* **2018**, *3*, 1165.

(13) Dai, B.; Li, K.; Shi, L.; Wan, X.; Liu, X.; Zhang, F.; Jiang, L.; Wang, S. Bioinspired Janus Textile with Conical Micropores for Human Body Moisture and Thermal Management. *Adv. Mater.* **2019**, *31*, 1904113.

(14) Si, Y.; Chen, L.; Yang, F.; Guo, F.; Guo, Z. Stable Janus superhydrophilic/hydrophobic nickel foam for directional water transport. *J. Colloid Interface Sci.* **2018**, *509*, 346−352.

(15) Yang, C.; Han, N.; Han, C.; Wang, M.; Zhang, W.; Wang, W.; Zhang, Z.; Li, W.; Zhang, X. Design of a Janus F-TiO2@PPS Porous Membrane with Asymmetric Wettability for Switchable Oil/Water Separation. *ACS Appl. Mater. Interfaces* **2019**, *11*, 22408−22418.

(16) Song, Y.; Zhou, J.; Fan, J. B.; Zhai, W.; Meng, J.; Wang, S. Hydrophilic/Oleophilic Magnetic Janus Particles for the Rapid and Efficient Oil−Water Separation. *Adv. Funct. Mater.* **2018**, *28*, 1802493.

(17) Lee, Y. S.; Kaang, B. K.; Han, N.; Lee, H.-J.; Choi, W. S. An anti-overturn Janus sponge with excellent floating stability for simultaneous pollutant remediation and oil/water separation. *J. Mater. Chem. A* **2018**, *6*, 16371−16381.

(18) Liu, Y. n.; Qu, R.; Zhang, W.; Li, X.; Wei, Y.; Feng, L. Lotus- and Mussel-Inspired PDA-PET/PTFE Janus Membrane: Toward Integrated Separation of Light and Heavy Oils from Water. *ACS Appl. Mater. Interfaces* **2019**, *11*, 20545−20556.

(19) Ren, F.; Li, G.; Zhang, Z.; Zhang, X.; Fan, H.; Zhou, C.; Wang, Y.; Zhang, Y.; Wang, C.; Mu, K.; Su, Y.; Wu, D. A single-layer Janus membrane with dual gradient conical micropore arrays for self-driving fog collection. *J. Mater. Chem. A* **2017**, *5*, 18403−18408.

(20) Zhou, H.; Zhang, M.; Li, C.; Gao, C.; Zheng, Y. Excellent Fog-Droplets Collector via Integrative Janus Membrane and Conical Spine with Micro/Nanostructures. *Small* **2018**, *14*, No. e1801335.

(21) Li, D.; Fan, Y.; Han, G.; Guo, Z. Multibioinspired Janus membranes with superwettable performance for unidirectional transportation and fog collection. *Chem. Eng. J.* **2021**, *404*, 126515.

(22) An, Y.-H.; Yu, S. J.; Kim, I. S.; Kim, S.-H.; Moon, J.-M.; Kim, S. L.; Choi, Y. H.; Choi, J. S.; Im, S. G.; Lee, K. E.; Hwang, N. S. Hydrogel Functionalized Janus Membrane for Skin Regeneration. *Adv. Healthcare Mater.* **2017**, *6*, 1600795.

(23) Ma, B.; Han, J.; Zhang, S.; Liu, F.; Wang, S.; Duan, J.; Sang, Y.; Jiang, H.; Li, D.; Ge, S.; Yu, J.; Liu, H. Hydroxyapatite nanobelt/polylactic acid Janus membrane with osteoinduction/barrier dual functions for precise bone defect repair. *Acta Biomater.* **2018**, *71*, 108−117.

(24) Wang, G.-J.; Wu, B.-H.; Xu, Z.-K.; Wan, L.-S. Janus polymer membranes prepared by single-side polydopamine deposition for dye adsorption and fine bubble aeration. *Mater. Chem. Front.* **2019**, *3*, 2102−2109.

(25) Shirsath, G. B.; Muralidhar, K.; Pala, R. G. S.; Ramkumar, J. Condensation of water vapor underneath an inclined hydrophobic textured surface machined by laser and electric discharge. *Appl. Surf. Sci.* **2019**, *484*, 999−1009.

(26) Može, M.; Senegačnik, M.; Gregorčič, P.; Hočevar, M.; Zupančič, M.; Golobič, I. Laser-Engineered Microcavity Surfaces with a Nanoscale Superhydrophobic Coating for Extreme Boiling Performance. *ACS Appl. Mater. Interfaces* **2020**, *12*, 24419−24431.

(27) Ding, Q.; Wang, L.; Hu, L. Tribology optimization by laser surface texturing: From bulk materials to surface coatings. *Laser Surface Engineering*; Woodhead Publishing, 2015; pp 405−422.

(28) Petkovšek, M.; Hočevar, M.; Gregorčič, P. Surface functionalization by nanosecond-laser texturing for controlling hydrodynamic cavitation dynamics. *Ultrason. Sonochem.* **2020**, *67*, 105126.

(29) Li, J.; Zhou, Y.; Wang, W.; Xu, C.; Ren, L. Superhydrophobic Copper Surface Textured by Laser for Delayed Icing Phenomenon. *Langmuir* **2020**, *36*, 1075−1082.

(30) Lu, Z.; Li, Y.; Lei, X.; Liu, J.; Sun, X. Nanoarray based "superaerophobic" surfaces for gas evolution reaction electrodes. *Mater. Horiz.* **2015**, *2*, 294−298.

(31) Semmens, M. J.; Gulliver, J. S.; Anderson, A. An Analysis of Bubble Formation Using Microporous Hollow Fiber Membranes. *Water Environ. Res.* **1999**, *71*, 307−315.

(32) Yu, C.; Zhang, P.; Wang, J.; Jiang, L. Superwettability of Gas Bubbles and Its Application: From Bioinspiration to Advanced Materials. *Adv. Mater.* **2017**, *29*, 1703053.

(33) Zheng, L.; Yapa, P. D. Buoyant Velocity of Spherical and Nonspherical Bubbles/Droplets. *J. Hydraul. Eng.* **2000**, *126*, 852−854.

https://doi.org/10.1021/acs.langmuir.1c00437
Langmuir 2021, 37, 6947−6952